Celestial Mech Dyn Astr (2006) 96:289–309
DOI 10.1007/s10569-006-9047-4

ORIGINAL ARTICLE

A sixth-order accurate scheme for solving two-point boundary value problems in astrodynamics

Roberto Armellin · Francesco Topputo

Received: 20 October 2005 / Revised: 22 May 2006 /
Accepted: 25 July 2006 / Published online: 27 October 2006

Abstract A sixth-order accurate scheme is presented for the solution of ODE systems supplemented by two-point boundary conditions. The proposed integration scheme is a linear multi-point method of sixth-order accuracy successfully used in fluid dynamics and implemented for the first time in astrodynamics applications. A discretization molecule made up of just four grid points attains a $O(h^6)$ accuracy which is beyond the first Dahlquist's stability barrier. Astrodynamics applications concern the computation of libration point halo orbits, in the restricted three- and four-body models, and the design of an optimal control strategy for a low thrust libration point mission.

Keywords Non-linear boundary value problem · Restricted three-body problem · Bicircular four-body problem · Halo orbits

1 Introduction

Two-point boundary value problems (TPBVPs) appear frequently in astrodynamics when solving a system of ordinary differential equations (ODEs) with boundary conditions on both sides of the integration interval is required. A typical example occurs in preliminary mission analysis in the frame of the two-body problem, in which an arc linking two fixed points in a given time is required—the classic Lambert's problem. Such a problem can be solved by using efficient semi-analytical algorithms since an analytic solution is available in the case of Kepler's problem (Battin 1987). Another example of TPBVP is solving an optimal control problem: the full system, made up by the states and the Lagrange multipliers dynamics, must be solved by respecting generic initial and final conditions derived by problem requirements. This kind of

R. Armellin · F. Topputo (✉)
Aerospace Engineering Department, Politecnico di Milano,
Via La Masa 34, 20156, Milano, Italy
e-mail: topputo@aero.polimi.it

problem is typically difficult to solve due to the doubled dimension of the system, the non-linear behavior of the Lagrange multipliers and their non-physical meaning, which frequently results in the lack of an appropriate initial guess.

Numerical methods for solving initial value problems (IVPs) are more developed than methods for solving BVPs. The latter are usually solved employing simple or multiple shooting schemes, in which the boundary value problem is divided into several IVPs to be solved within each subinterval. Such methods can reach effective convergence but are highly sensitive to intermediate initial conditions when the subintervals become large. The technique proposed in this paper belongs to a class called *difference methods* according to the standard classification of Stoer and Bulirsch (1993) which are based on the discretization of first-order ODEs over an appropriate grid. The resulting finite-dimensional problem, satisfying both the defects, resulting by the discretization process, and the boundary conditions, is solved. In this paper, we present a method which can solve a large class of BVPs and apply it for the first time in astrodynamics.

Quartapelle and Rebay (1990) developed a discretization strategy based on linear approximations of both sides of the first-order system of differential equations, similar to the linear multi-step methods in solving IVPs. The discrete approximations of the two-point boundary value problems is made to embody the fundamental theorem of differential calculus, whose exact fulfillment is reproduced at the level of the discrete equations. This is achieved by retaining a discrete representation of the entire problem, consisting of the equations and supplementary conditions, by means of discrete equations linking the unknowns at all grid points. The presence of this special equation involving the discrete unknowns gives to the method an intrinsically implicit character: hence the name linear multi-*point* method, to underline the difference with respect to the time-*marching* nature of the linear multi-step schemes for initial value problems. In its original presentation this method was of fourth- and sixth-order accuracy and involved four and six grid points at each discretization interval, respectively.

Recently, Quartapelle and Scandroglio (2003) have implemented a new linear multi-point scheme, following a suggestion of Paolo Luchini, to reach sixth-order accuracy with improved computational efficiency. This new scheme resorts to four grid points instead of six to attain an accuracy beyond the first Dahlquist's stability barrier. This formulation gives rise to an algebraic system characterized by a bordered quadri-diagonal matrix that can be easily factorized. This new method has been successively applied in fluid dynamics to determine the multiple solutions of the Falkner–Skan equation for normal and reverse flows.

The sixth-order linear multi-point method (LMPM) of Quartapelle and Scandroglio has been revised and applied to BVPs in astrodynamics. The core of the method has been preserved and described throughout the paper for the sake of clarity. As a counterpoint, the computation of periodic orbits, for which the final time is unknown, has required a further improvement. The original dynamical system has been rearranged by introducing a new independent variable and adding an auxiliary differential equation for the final time. This allows us in computing the L_1 and L_2 halo orbits appearing in the three-body problem with the Earth and Moon as primaries. We then analyze how these orbits behave when the gravitational attraction of the Sun is taken into account. In the latter case, an exceptional behavior occurs around the L_2 point, where there is a strong effect due to the 2:1 resonance between the frequency of the halo orbits and the synodical frequency of the Sun in the Earth–Moon system (Masdemont and Mondelo 2004). This effect causes a sort of "breakage" in the periodicity of halo

orbits. Even if periodic solutions are found for a specific phase of the Sun, we will talk about *quasi-periodic* halo orbits because the periodicity is lost in successive times as the Sun moves in its circular orbit. Finally, a more complicated BVP, concerning the design of an optimal control strategy for a low thrust libration point mission is solved.

This paper is organized as follows. The next section illustrates the problem statements: the equations of the restricted three-body problem (R3BP) and the restricted four-body problem (R4BP) with their respective boundary conditions. Then the Euler–Lagrange equations and the boundary conditions are derived for the optimal control case. In Sect. 3 we reproduce the construction of the sixth-order accurate method for discretizing a general dynamics in first-order form. Then the Newton's method for the iterative solution to a system of non-linear algebraic equations is illustrated. In Sect. 4 we show the solutions to the above problems obtained by the $O(h^6)$ LMPM. In the Appendix, the algorithmic flow chart of the method and the block bordered quadri-diagonal profile of the matrix corresponding to the discretization scheme are reported.

2 Problem statement

In this section the systems of ODEs to be solved with LMPM are described; for a detailed derivation of the equations of motion, refer to Szebehely (1967) for R3BP, Simó et al. (1995) for R4BP, and Bryson and Ho (1975) for the necessary conditions of the optimal control problem.

2.1 Restricted three-body problem

The differential equations describing the motion of a negligible mass under the gravitational attraction of the Earth and the Moon (primaries) are written in a synodic reference frame

$$\ddot{x} - 2\dot{y} = \frac{\partial \Omega_3}{\partial x}, \quad \ddot{y} + 2\dot{x} = \frac{\partial \Omega_3}{\partial y}, \quad \ddot{z} = \frac{\partial \Omega_3}{\partial z}, \tag{1}$$

in which the three-body centrifugal–gravitational potential function is

$$\Omega_3(x, y, z) = \frac{1}{2}(x^2 + y^2) + \frac{1-\mu}{r_1} + \frac{\mu}{r_2} + \frac{1}{2}\mu(1-\mu), \tag{2}$$

and (x, y, z) are the co-ordinates of the spacecraft. System of equations (1) is written in dimensionless units that set the sum of the masses of the primaries, their distance, and their angular velocity equal to one. The Moon has mass μ and is located at $(1-\mu, 0, 0)$ while the Earth has mass $1-\mu$ and is placed at $(-\mu, 0, 0)$. The mass parameter used for the Earth–Moon problem is $\mu = 0.01215\,0582$. The distances in Eq. 2 are

$$r_1^2 = (x+\mu)^2 + y^2 + z^2, \quad r_2^2 = (x-1+\mu)^2 + y^2 + z^2. \tag{3}$$

Dynamical system (1) presents five points of equilibrium. Three points L_1, L_2 and L_3, called *collinear*, are aligned with the primaries; the L_4 and L_5 points, called *triangular*, are at the vertex of two equilateral triangles with the primaries. In a linear analysis collinear points behave like the product of a saddle $\times$ a 4D center, and this paper is mostly focused on the L_1 and L_2 periodic orbits arising from the presence of the center part. This region, indeed, is characterized by the presence of planar and

vertical Lyapunov orbits, three-dimensional halo and quasi-halo orbits, and Lissajous trajectories. Halo orbits are large orbits with equal in-plane and out-of-plane frequencies. Such orbits are usually obtained by means of a simple shooting method which corrects a third-order analytic first guess obtained by expanding in power series the gravitational terms in Eq. 2; this procedure is called the "Richardson method" (Richardson 1980; Thurman and Worfolk 1996). A more refined process consists of expanding the gravitational terms up to an arbitrary order, using the Lindstedt–Poincaré method, and then correcting this initial guess in a complete ephemeris model with a multiple shooting technique; this is the method used by the "Barcelona group" (Masdemont 2005; Gómez et al. 2000).

In this paper, the developed $O(h^6)$ LMPM is used to correct a first guess obtained by means of a third order analytical solution. These corrections are carried out both under three- and four-body dynamics.

2.2 Restricted four-body problem

When the presence of the Sun is taken into account, the resulting dynamical system is no longer autonomous since the Sun does not have a fixed position in the synodic system. In order to make the system autonomous, an additional "clock" equation must be added to system (1) (Yagasaki 2004)

$$\ddot{x} - 2\dot{y} = \frac{\partial \Omega_4}{\partial x}, \quad \ddot{y} + 2\dot{x} = \frac{\partial \Omega_4}{\partial y}, \quad \ddot{z} = \frac{\partial \Omega_4}{\partial z}, \qquad \dot{\theta} = \omega_S, \tag{4}$$

in which the potential function accounts for the gravitational attraction given by the presence of the Sun

$$\Omega_4(x, y, z, \theta) = \Omega_3(x, y, z) + \frac{m_S}{r_3} - \frac{m_S}{\rho^2}(x \cos\theta + y \sin\theta). \tag{5}$$

The dimensionless physical parameters of the Sun are assumed to be in agreement with the rotating and normalized Earth–Moon system introduced in Sect. 2.1. The distance between the Sun and the Earth–Moon barycenter corresponds to $\rho = 3.8881 \times 10^2$, the mass of the Sun is $m_S = 3.2890 \times 10^5$, and its angular velocity with respect to the Earth–Moon synodic system is $\omega_S = -0.9251$. With these constants the co-ordinates of the Sun are given by $\{\rho \cos\theta, \rho \sin\theta, 0\}^T$ and so the Sun–spacecraft distance is

$$r_3^2 = (x - \rho \cos\theta)^2 + (y - \rho \sin\theta)^2 + z^2. \tag{6}$$

Note that the bicircular system (4) is *not* coherent because the primaries do not respect Newton's equations. However, it is expected to be a good approximation of the real four-body dynamics because the Earth and Moon eccentricity is equal to 0.016 and 0.054, respectively, and the Moon's orbit is inclined to the ecliptic by only 5°.

2.3 First-order reduction and periodicity conditions

In solving a boundary value problem using LMPM, the equations of motion, either those describing the three- or the four-body dynamics, must be written in the generic first-order form

$$\dot{\mathbf{y}} = \mathbf{f}(t, \mathbf{y}). \tag{7}$$

It is straightforward that the states $\mathbf{y}$ and the vector field $\mathbf{f}$ have a different meaning for the two models discussed; in the R3BP

$$\begin{aligned}\mathbf{y} &= \{x,\ y,\ z,\ v_x,\ v_y,\ v_z\}^T,\\ \mathbf{f} &= \left\{v_x,\ v_y,\ v_z,\ 2v_y + \frac{\partial \Omega_3}{\partial x},\ -2v_x + \frac{\partial \Omega_3}{\partial y},\ \frac{\partial \Omega_3}{\partial z}\right\}^T,\end{aligned} \tag{8}$$

while in the bicircular R4BP

$$\begin{aligned}\mathbf{y} &= \{x,\ y,\ z,\ v_x,\ v_y,\ v_z,\ \theta\}^T,\\ \mathbf{f} &= \left\{v_x,\ v_y,\ v_z,\ 2v_y + \frac{\partial \Omega_4}{\partial x},\ -2v_x + \frac{\partial \Omega_4}{\partial y},\ \frac{\partial \Omega_4}{\partial z},\ \omega_S\right\}^T.\end{aligned} \tag{9}$$

When the final time (i.e. the period) is unknown, the first-order form (7) is not suitable to solve BVP, as the computation of halo orbits. In this case a time scale change could be completed by setting $t = T\tau$, in which T is the final time (an unknown constant) and $0 \leq \tau \leq 1$ is the new independent variable. The dynamical system with the unknown variables $\mathbf{y} = \mathbf{y}(\tau)$ and $T = T(\tau)$ becomes

$$\begin{cases}\dfrac{\mathrm{d}\mathbf{y}}{\mathrm{d}\tau} = T\,\mathbf{f}(\tau, \mathbf{y})\\ \dfrac{\mathrm{d}T}{\mathrm{d}\tau} = 0\end{cases}. \tag{10}$$

Note that system (10) must be integrated within the interval $[0, 1]$. The period T becomes an unknown of the differential system itself and, as for $\mathbf{y}(\tau)$, its value is given once the BVP is solved. An additional boundary condition must be supplied to solve system (10) since the unknown vector is now $\widetilde{\mathbf{y}} = \{\mathbf{y}, T\}^T$. System (10) can be rewritten into the first-order compact form (7) as $\dot{\widetilde{\mathbf{y}}} = \widetilde{\mathbf{f}}(\tau, \widetilde{\mathbf{y}})$, with $\widetilde{\mathbf{f}} = \{T\mathbf{f}, 0\}^T$. Note that the unknown final time formulation further increases the non-linearity of the vector field, and so the BVP becomes more sensitive to the initial guess and more difficult to solve.

2.4 Boundary conditions for halo orbits

With $\mathbf{y}(t_0)$ and $\mathbf{y}(t_f)$ equal to the unknown $\mathbf{y} = \{x, y, z, v_x, v_y, v_z\}^T$ evaluated at the initial and final times t_0 and t_f, respectively, the periodicity condition is $\mathbf{y}(t_0) = \mathbf{y}(t_f)$. The unknown final time formulation, which is used to compute halo orbits, requires one more boundary condition to find the orbital period. Hence, in the formalism of (10), the boundary conditions for a T-periodic orbit become

$$\begin{cases}\mathbf{y}(0) - \mathbf{y}(1) = 0\\ \qquad T(0) = T.\end{cases} \tag{11}$$

A more interesting application concerns the possibility of prescribing a geometrical dimension of the periodic orbit. This is the case of the out-of-plane amplitude A_z used to design the best orbit that is suitable for a mission, making the boundary conditions

$$\begin{cases}\mathbf{y}(0) - \mathbf{y}(1) = 0\\ \qquad z(0) = A_z.\end{cases} \tag{12}$$

The boundary conditions for the computation of quasi-periodic halo orbits in the R4BP are

$$\begin{cases} \mathbf{y}(0) - \mathbf{y}(1) = 0 \\ \theta(0) = \theta_0 \\ z(0) = A_z, \end{cases} \tag{13}$$

in which the initial phase of the Sun θ_0 must be prescribed to let system (9) to be supplemented by eight boundary conditions.

2.5 Low thrust optimal transfer to halo orbits

The *controlled* R3BP

$$\ddot{x} - 2\dot{y} = \frac{\partial \Omega_3}{\partial x} + u_1, \quad \ddot{y} + 2\dot{x} = \frac{\partial \Omega_3}{\partial y} + u_2, \quad \ddot{z} = \frac{\partial \Omega_3}{\partial z} + u_3, \tag{14}$$

can be rewritten in the first order form as

$$\dot{\mathbf{y}} = \mathbf{f}(\mathbf{y}, \mathbf{u}), \tag{15}$$

in which $\mathbf{u} = \{u_1, u_2, u_3\}^T$ and $\mathbf{y} = \{x, y, z, v_x, v_y, v_z\}^T$ are the control and state vectors, respectively. We aim at minimizing the objective function

$$J = \int_{t_0}^{t_f} L(\mathbf{y}, \mathbf{u}, t)\, \mathrm{d}t = \frac{1}{2} \int_{t_0}^{t_f} \mathbf{u}^T \mathbf{u}\, \mathrm{d}t, \tag{16}$$

with prescribed initial and final conditions $\mathbf{y}_0$ and $\mathbf{y}_f$ on the states and within the time interval $[t_f, t_0]$. Introducing the Lagrange multipliers λ_i, $i = 1, \ldots, 6$, the Euler–Lagrange equations read

$$\dot{\mathbf{y}} = \frac{\partial H}{\partial \boldsymbol{\lambda}}, \quad \dot{\boldsymbol{\lambda}} = -\frac{\partial H}{\partial \mathbf{y}}, \quad 0 = \frac{\partial H}{\partial \mathbf{u}}, \tag{17}$$

in which $H = \boldsymbol{\lambda}^T \mathbf{f} + L$ is the Hamiltonian of the optimal control problem. System (17) represents a set of differential algebraic equations (DAEs) to be solved by substitution exploiting the last equation which provides the values of the control functions in terms of Lagrange multipliers

$$u_i = -\lambda_{3+i}, \qquad i = 1, 2, 3. \tag{18}$$

Hence, system (17) must be solved together with the following 12 boundary conditions

$$\begin{cases} \mathbf{y}(t_0) = \mathbf{y}_0 \\ \mathbf{y}(t_f) = \mathbf{y}_f. \end{cases} \tag{19}$$

Solving system (17) with boundary conditions (19) means finding the functions $\mathbf{y} = \mathbf{y}(t)$ and $\boldsymbol{\lambda} = \boldsymbol{\lambda}(t)$ for $t \in [t_0, t_f]$; then, with relation (18), the set of optimal control functions $\mathbf{u} = \mathbf{u}(t)$ is derived. This problem is difficult to solve due to the high non-linearities of the dynamics of the Lagrange multipliers. Their lack of physical meaning makes it difficult to find an appropriate initial guess close to the final solution.

3 Sixth-order linear multi-point method

In this section we report the sixth-order LMPM for the solution of the BVPs stated above (Quartapelle and Scandroglio 2003). We refer to the generic n first-order equations

$$\dot{\mathbf{y}} = \mathbf{f}(t, \mathbf{y}), \tag{20}$$

supplemented by the appropriate n boundary conditions that are assumed to be of the general non-linear form

$$\mathbf{g}(\mathbf{y}(t_a), \mathbf{y}(t_b)) = 0. \tag{21}$$

The problem is to solve (20) and (21) within a finite time interval $[t_a, t_b]$, over a uniform grid consisting of N points so that the step size of the discretization is

$$h = \Delta t = \frac{t_b - t_a}{N - 1}, \tag{22}$$

with the grid points defined by $t_i = t_a + (i - 1)h$, for $i = 1, \ldots, N$.

The problem is now discretized by a strategy akin to that classically adopted to solve initial value problems for ODEs, namely, the *linear multi-step method*. Due to the non-initial-value character of the first-order system associated with a boundary value problem, only central difference approximations are applied. Constructed below is the sixth-order accurate method belonging to the class of schemes called *linear multi-point methods* to be distinguished from those developed for the time integration of initial value problems.

3.1 Construction of the sixth-order accurate scheme

The sixth-order linear multi-point method is obtained by approximating the differential system (20) at midpoints $t_{i+1/2}$, $i = 2, \ldots, N - 2$, by means of a general computational molecule involving four points and of two special molecules involving five points at the both ends of the integration interval, as illustrated by the following scheme. In the figure, the • denotes the grid point of the computational molecules involved in the discretization while the ◇ indicates the location chosen for the discrete approximation of the equations.

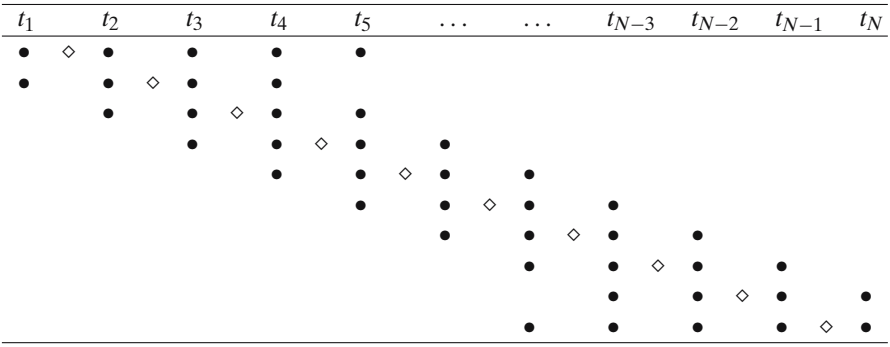

For the first special molecule associated with the left extreme, the relation expressing the linear approximation to a scalar equation $\mathrm{d}y/\mathrm{d}t = f(t, y)$ based on five points is given by

$$\begin{aligned}&\hat{\alpha}_1 y_1 + \hat{\alpha}_2 y_2 + \hat{\alpha}_3 y_3 + \hat{\alpha}_4 y_4 + \hat{\alpha}_5 y_5 \\ &\quad = h(\hat{\beta}_1 f_1 + \hat{\beta}_2 f_2 + \hat{\beta}_3 f_3 + \hat{\beta}_4 f_4 + \hat{\beta}_5 f_5),\end{aligned} \tag{23}$$

in which $f_i = f(t_i, y_i)$. Generally, for any internal molecule with midpoint $t_{i+1/2}$, the linear discretization based on four points is

$$\begin{aligned}&\alpha_1 y_{i-1} + \alpha_2 y_i + \alpha_3 y_{i+1} + \alpha_4 y_{i+2} \\ &\quad = h(\beta_1 f_{i-1} + \beta_2 f_i + \beta_3 f_{i+1} + \beta_4 f_{i+2}).\end{aligned} \tag{24}$$

A special molecule using five points analogous to that in (23) is used at the right end of the interval, leading to a total of $N - 1$ discrete equations approximating the first-order dynamical system. The α_i and β_i coefficients are now determined by imposing cancellation conditions that enforce the *exact respect* of the *fundamental theorem of calculus* at the level of the discrete equations, according to the method followed in Quartapelle and Scandroglio (2003). After some computations, the values of the coefficients of the linear approximation are, for the two special five-point molecules

$$\begin{cases} \hat{\alpha}_1 = -\dfrac{49}{60}, & \hat{\alpha}_2 = \dfrac{38}{60}, & \hat{\alpha}_3 = \dfrac{11}{60}, & \hat{\alpha}_4 = 0, & \hat{\alpha}_5 = 0, \\ \hat{\beta}_1 = \dfrac{403}{1440}, & \hat{\beta}_2 = \dfrac{591}{720}, & \hat{\beta}_3 = -\dfrac{11}{60}, & \hat{\beta}_4 = \dfrac{73}{720}, & \hat{\beta}_5 = -\dfrac{27}{1440}, \end{cases} \tag{25}$$

and, for the general four-point molecule,

$$\begin{cases} \alpha_1 = -\dfrac{11}{60}, & \alpha_2 = -\dfrac{27}{60}, & \alpha_3 = \dfrac{27}{60}, & \alpha_4 = \dfrac{11}{60}, \\ \beta_1 = \dfrac{1}{20}, & \beta_2 = \dfrac{9}{20}, & \beta_3 = \dfrac{9}{20}, & \beta_4 = \dfrac{1}{20}. \end{cases} \tag{26}$$

Thus, the five-point molecule assumes the form

$$\begin{aligned}&-\frac{49}{60} y_1 + \frac{38}{60} y_2 + \frac{11}{60} y_3 \\ &\quad = h\left(\frac{403}{1440} f_1 + \frac{591}{720} f_2 - \frac{11}{60} f_3 + \frac{73}{720} f_4 - \frac{27}{1440} f_5\right),\end{aligned} \tag{27}$$

and the general four-point molecule is instead

$$\begin{aligned}&-\frac{11}{60} y_{i-1} - \frac{27}{60} y_i + \frac{27}{60} y_{i+1} + \frac{11}{60} y_{i+2} \\ &\quad = h\left(\frac{1}{20} f_{i-1} + \frac{9}{20} f_i + \frac{9}{20} f_{i+1} + \frac{1}{20} f_{i+2}\right).\end{aligned} \tag{28}$$

For completeness, let us explicitly write the set of computational molecules which involve the first grid points. Replacing $\hat{\alpha}_i$ and α_i through (25) and (26), the left hand side of the discrete equations becomes the following scheme

$$
\begin{array}{ccccccc}
-\frac{49}{60}y_1 & \frac{38}{60}y_2 & \frac{11}{60}y_3 & 0 & 0 & & \\
-\frac{11}{60}y_1 & -\frac{27}{60}y_2 & \frac{27}{60}y_3 & \frac{11}{60}y_4 & & & \\
 & -\frac{11}{60}y_2 & -\frac{27}{60}y_3 & \frac{27}{60}y_4 & \frac{11}{60}y_5 & & \\
 & & -\frac{11}{60}y_3 & -\frac{27}{60}y_4 & \frac{27}{60}y_5 & \ddots & \\
 & & & -\frac{11}{60}y_4 & -\frac{27}{60}y_5 & \ddots & \\
 & & & & -\frac{11}{60}y_5 & \ddots & \\
 & & & & & \ddots &
\end{array}
\tag{29}
$$

The summation of the coefficients in each column of this triangular matrix corresponds to "integrate" the left hand side of the discrete equations and therefore verifies the fundamental theorem of calculus, $\int_{t_a}^{t_b} \frac{\mathrm{d}y}{\mathrm{d}t}\mathrm{d}t = y(t_b) - y(t_a)$, because the sum of all elements in each column is zero except for the first column whose total is $-y_1 = -y(t_a)$. Analogously, the right hand side of the discrete equation is

$$
\begin{array}{ccccccc}
\frac{403}{1440}hf_1 & \frac{591}{720}hf_2 & -\frac{11}{60}hf_3 & \frac{73}{720}hf_4 & -\frac{27}{1440}hf_5 & & \\
\frac{1}{20}hf_1 & \frac{9}{20}hf_2 & \frac{9}{20}hf_3 & \frac{1}{20}hf_4 & & & \\
 & \frac{1}{20}hf_2 & \frac{9}{20}hf_3 & \frac{9}{20}hf_4 & \frac{1}{20}hf_5 & & \\
 & & \frac{1}{20}hf_3 & \frac{9}{20}hf_4 & \frac{9}{20}hf_5 & \ddots & \\
 & & & \frac{1}{20}hf_4 & \frac{9}{20}hf_5 & \ddots & \\
 & & & & \frac{1}{20}hf_5 & \ddots & \\
 & & & & & \ddots &
\end{array}
\tag{30}
$$

It is worth noting that the summation of the $\hat{\beta}_i$ and β_i in the scheme (30) leads to an approximation of the definite integral coincident with the Gregory quadrature formula of precision $O(h^6)$. Gregory formulas provide the natural numerical quadrature for a known discrete function on a uniform grid. In those formulas, the weight is constant at internal points except for those near to the ends of the integration interval where end corrections are applied (Fox 1957).

After discretizing the problem over a uniform grid of N points, $N-1$ discrete equations in the scalar case could be derived because they correspond to the number of integration sub-intervals. The N-th equation, which allows one to solve the algebraic problem, is obtained through the (scalar) boundary condition.

One feature of the sixth-order LMPM is that it attains an accuracy beyond the first Dahlquist stability barrier (Lambert 1991). Dahlquist's theorem states that the order of accuracy q of a stable linear method based on p points (namely, $p-1$ steps), in the language of linear multi-step methods, satisfies

$$q \leq \begin{cases} p-1 & \text{if the method is explicit,} \\ p & \text{if } p \text{ is even,} \\ p+1 & \text{if } p \text{ is odd.} \end{cases}$$

The present $O(h^6)$ Linear Multi-Point discretization is implicit and its general molecule has $p = 4$ points; therefore, from Dahlquist's theorem the highest order of accuracy attainable by the new method is expected to be $q = p = 4$ while the construction guarantees an order of accuracy of six. The point is that the theorem pertains to linear multi-step methods for IVPs while the proposed $O(h^6)$ accurate method is established to solve BVPs, although expressed as a first-order system. In fact, the LMPM is characterized by the presence of a (block) row, to enforce the two-point boundary conditions, which contains non-zero elements either in both the first and last block or along the entire row. It is the occurrence of this special row that allows the method with only four points to reach the sixth-order accuracy and therefore to overcome the first Dahlquist stability barrier. Note that Quartapelle and Rebay (1990) introduced fourth-order and sixth-order LMPM based on computational molecules with four and six points, respectively. Thus, the accuracy of the two old schemes was within Dahlquist's barrier and required a greater computational effort. On the contrary, the present method reaches an $O(h^6)$ accuracy involving just four points. As a result, a better computational efficiency is gained since fewer function evaluations are needed, and an increased sparsity of the discretization matrix is reached.

3.2 Newton's method for the block non-linear system

After discretization by LMPM, a set of n ODEs on a uniform grid of N points, $n(N-1)$ algebraic equations are generated and the unknown vector function $\mathbf{y}(t)$ is represented by a set of nN discrete values. The two nN column vectors are

$$\mathbb{Y} = \begin{pmatrix} \mathbf{y}_1 \\ \mathbf{y}_2 \\ \cdot \\ \cdot \\ \cdot \\ \mathbf{y}_N \end{pmatrix} = \begin{pmatrix} \begin{pmatrix} y_{1,1} \\ y_{2,1} \\ \cdot \\ y_{n,1} \end{pmatrix} \\ \cdot \\ \cdot \\ \cdot \\ \begin{pmatrix} y_{1,N} \\ y_{2,N} \\ \cdot \\ y_{n,N} \end{pmatrix} \end{pmatrix} \quad \text{and} \quad \mathbb{F}(\mathbb{Y}) = \begin{pmatrix} \mathbf{f}(t_1, \mathbf{y}_1) \\ \mathbf{f}(t_2, \mathbf{y}_2) \\ \cdot \\ \cdot \\ \cdot \\ \mathbf{f}(t_N, \mathbf{y}_N) \end{pmatrix} = \begin{pmatrix} \begin{pmatrix} f_{1,1} \\ f_{2,1} \\ \cdot \\ f_{n,1} \end{pmatrix} \\ \cdot \\ \cdot \\ \cdot \\ \begin{pmatrix} f_{1,N} \\ f_{2,N} \\ \cdot \\ f_{n,N} \end{pmatrix} \end{pmatrix}. \tag{31}$$

Thus, the LMPM approximation of this problem leads to the following non-linear system of $n(N-1)$ algebraic equations

$$A\mathbb{Y} = hB\mathbb{F}(\mathbb{Y}), \tag{32}$$

in which A and B denote two $n(N-1) \times nN$ matrices filled by the coefficients $\hat{\alpha}_i$, α_i and $\hat{\beta}_i$, β_i, respectively. The problem is well posed when the n non-linear two-point conditions (21) are included. In the frame of the discretization strategy introduced so far, such equations can be rewritten in the form $\mathbf{g}(\mathbf{y}_1, \mathbf{y}_N) = 0$, or more generally $\mathbf{g}(\mathbb{Y}) = 0$, including also integral boundary conditions. The resulting nN system can be solved by means of Newton's method. To this aim, let us define

$$\boldsymbol{\varphi}(\mathbb{Y}) \equiv \{\mathbf{g}(\mathbb{Y}), A\mathbb{Y} - hB\mathbb{F}(\mathbb{Y})\}^T, \tag{33}$$

so that the non-linear system of equations is written as

$$\boldsymbol{\varphi}(\mathbb{Y}) = 0. \tag{34}$$

Note that the nature of the boundary conditions, either linear, non-linear or integral, would not affect the generic non-linear nature of (34). Dealing with non-linear dynamics results in non-linear discretized system of algebraic equation (32) and the inclusion of the boundary conditions has a little impact on (33). This feature has been proven in Quartapelle and Rebay (1990) in which different sets of boundary conditions have been analyzed.

Assuming an initial guess $\mathbb{Y}_0$ is given, its correction $\Delta\mathbb{Y}_0$ defined by Newton's method in incremental form is given by expanding $\boldsymbol{\varphi}(\mathbb{Y}_0 + \Delta\mathbb{Y}_0)$ around $\mathbb{Y}_0$ by the Taylor series to the first order

$$\boldsymbol{\varphi}(\mathbb{Y}_0 + \Delta\mathbb{Y}_0) \approx \boldsymbol{\varphi}(\mathbb{Y}_0) + \mathbb{J}(\mathbb{Y}_0)\Delta\mathbb{Y}_0 = 0, \tag{35}$$

in which

$$\mathbb{J}(\mathbb{Y}) \equiv \frac{\partial\boldsymbol{\varphi}(\mathbb{Y})}{\partial\mathbb{Y}} = \begin{bmatrix} \dfrac{\partial\mathbf{g}(\mathbb{Y})}{\partial\mathbb{Y}} \\ A - hB\dfrac{\partial\mathbb{F}(\mathbb{Y})}{\partial\mathbb{Y}} \end{bmatrix}. \tag{36}$$

By solving Eq. 35 with respect to $\Delta\mathbb{Y}_0$, we find

$$\Delta\mathbb{Y}_0 = -[\mathbb{J}(\mathbb{Y}_0)]^{-1}\boldsymbol{\varphi}(\mathbb{Y}_0), \tag{37}$$

and the new approximate solution $\mathbb{Y}_1$ is

$$\mathbb{Y}_1 = \mathbb{Y}_0 + \gamma\Delta\mathbb{Y}_0 = \mathbb{Y}_0 - \gamma[\mathbb{J}(\mathbb{Y}_0)]^{-1}\boldsymbol{\varphi}(\mathbb{Y}_0). \tag{38}$$

A full step of the Newton iteration is taken by setting $\gamma = 1$, otherwise a step size control can be introduced by taking $0 < \gamma < 1$ allowing the method to include a form of continuation to ease the convergence in though problems. The linear system to be solved at the first iteration assumes the form

$$\mathbb{A}_0\Delta\mathbb{Y}_0 = -\boldsymbol{\varphi}(\mathbb{Y}_0), \quad \text{with} \qquad \mathbb{A}_0 = \begin{bmatrix} \dfrac{\partial\mathbf{g}(\mathbb{Y})}{\partial\mathbb{Y}} \\ A - hB\dfrac{\partial\mathbb{F}(\mathbb{Y})}{\partial\mathbb{Y}} \end{bmatrix}_{\mathbb{Y}=\mathbb{Y}_0}. \tag{39}$$

Note that the nN-order Jacobian $\mathbb{A}_0$ can be computed either analytically evaluating the derivatives of both the vector field and the boundary condition, or numerically with a finite-difference approximation. Thus, the UL factorization $\mathbb{A}_0 = \mathbb{U}_0\mathbb{L}_0$ is used to determine the new iterate by means of the substitutions

$$\Delta\mathbb{Y}_0 = -\mathbb{L}_0^{-1}\mathbb{U}_0^{-1}\boldsymbol{\varphi}(\mathbb{Y}_0). \tag{40}$$

This is the solution to the linear system for the first step, while the incremental unknown $\Delta\mathbb{Y}_k$ for any subsequent iteration with $k \geq 0$ is given by the relation

$$\Delta\mathbb{Y}_k = -\mathbb{L}_k^{-1}\mathbb{U}_k^{-1}\boldsymbol{\varphi}(\mathbb{Y}_k), \tag{41}$$

in which $\mathbb{U}_k\mathbb{L}_k = \mathbb{A}_k$. Iterations terminate when the relative or the absolute norm of the corrections is below the acceptable tolerance ε

$$\frac{\|\Delta\mathbb{Y}_k\|}{\|\mathbb{Y}_k\|} \leq \varepsilon \quad \text{if } \|\mathbb{Y}_k\| \geq 1 \quad \text{or} \quad \|\Delta\mathbb{Y}_k\| \leq \varepsilon \quad \text{if } \|\mathbb{Y}_k\| < 1. \tag{42}$$

For completeness the algorithmic flow chart, the block bordered quadri-diagonal profile of the matrix $\mathbb{A}_k$, and the factorized triangular matrixes $\mathbb{L}_k$ and $\mathbb{U}_k$ are reported in Appendix.

4 Astrodynamics applications

All the results shown in this section concern the R3BP with the Earth and Moon as primaries; when the Sun perturbation is accounted for, we refer to the R4BP as discussed in Sect. 2.2. Periodic halo orbits are located about L_1 and L_2 equilibrium points. Once the BVP is solved, the solution is further assessed with a RKF78 integrator which solves the IVP with initial condition taken equal to the first grid point, with absolute and relative tolerance set to 10^{-10}. This integration scheme is eighth-order accurate and it is used to validate the solution that is sixth-order accurate. Algorithms have been written in MATLAB7 on a PC with a 2.6 GHz processor and 512 MB RAM.

4.1 Halo orbits in the R3BP

L_1 and L_2 halo orbits are easily computed with the LMPM starting by third-order analytical initial guesses. Figure 1a shows an L_1 periodic halo orbit with an out-of-plane amplitude equal to $Az = 8,000$ km obtained with boundary conditions (12). Figure 1b illustrates that the solution satisfies the boundary condition on the out-of-plane amplitude. This example has been computed using $N = 51$ points with convergence in four Newton iterations. The computational time is 0.20 s. Figure 2 illustrates the two families of halo orbits with amplitudes ranging from 1,000 to 20,000 km. Using either boundary conditions (11) or (12), these two families of orbits can be parameterized with T or A_z as parameter.

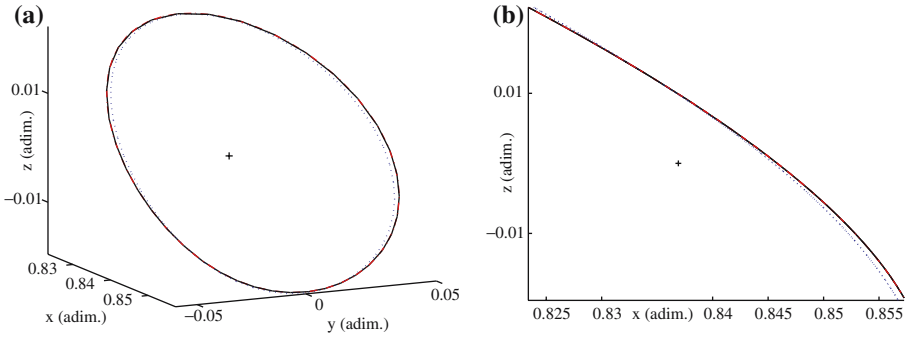

Fig. 1 An $Az = 8,000$ km L_1 halo orbit in the R3BP; third-order initial guess (dotted), LMPM solution (dash-dot) and RKF78 validation (solid). (**a**) 3D view; (**b**) (x, z) view

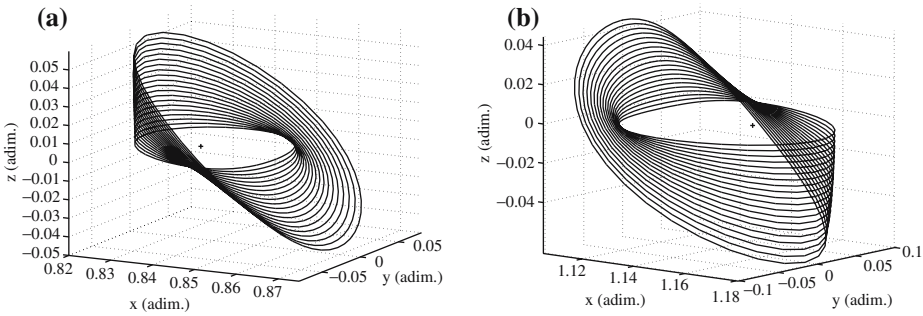

Fig. 2 Families of halo orbits around L_1 and L_2. (**a**) L_1 family; (**b**) L_2 family

4.2 Quasi-periodic halo orbits in the R4BP

If LMPM is applied to compute halo orbits in the Sun-perturbed R4BP assuming the third-order initial guess and the eight boundary conditions (13), the algorithm does not converge. This problem can be circumvented by observing that if the mass of the Sun m_S in Eq. 5 equals zero, the four-body dynamics degenerates into three-body dynamics described by system of equations (1). This means that if a halo orbit has been obtained in the R3BP, as the ones mentioned in the previous section, the parameter m_S could be slightly increased from zero to the final value $m_S = 3.2890 \times 10^5$. Several intermediate BVPs, with vector field (9), boundary conditions (13), and an initial guess equal to the solution at the previous step, can be solved. In this case the LMPM is able to converge. This process is called *numerical continuation* and the mass of the Sun is called *continuation parameter*.

Note once again that, even if a set of solutions satisfying boundary conditions (13) is found, they correspond to quasi-periodic orbits. Even though the values of position and the velocity coincide with those after one revolution, the Sun moving in its circular orbit will cause the loss of this periodicity with successive revolutions.

4.2.1 Numerical continuation of quasi-periodic halos in the R4BP

The problem stated in Sect. 2.4 for a definite value of m_S is addressed. The non-linear system of discrete equations for such a value is indicated by

$$\boldsymbol{\varphi}(\mathbb{Y}; m_S) = 0, \tag{43}$$

in which

$$\boldsymbol{\varphi}(\mathbb{Y}; m_S) = \{\mathbf{g}(\mathbb{Y}), A\,\mathbb{Y} - hB\,\mathbb{F}(\mathbb{Y}; m_s)\}^T. \tag{44}$$

As stated, the continuation method consists of solving a sequence of non-linear problems for different values of m_S approaching the true value of m_S gradually. To distinguish the q-th step of the continuation procedure, the following notation is used

$$\boldsymbol{\varphi}({}^q\mathbb{Y}; {}^q m_S) = 0, \tag{45}$$

and the procedure is completely defined by specifying the ${}^q m_S$ updating strategy.

As anticipated, the first step of the continuation procedure assumes $m_S = 0$, and the initial guess provided by the third-order expansion, is indicated by $\mathbb{Y}_{ig}$. Hence, the first problem to solve can be represented as

$$\begin{cases} {}^{1}m_S = 0 \\ {}^{1}\mathbb{Y}_0 = \mathbb{Y}_{ig} \\ \Phi({}^{1}\mathbb{Y}; {}^{1}m_S) = 0. \end{cases} \tag{46}$$

The subsequent steps of the numerical continuation procedure for $q = 2, 3, \ldots$ are performed by taking the solution ${}^{q-1}\mathbb{Y}$ of the previous step $q-1$ as the initial guess for the Newton iteration. The problem at step q is stated by

$$\begin{cases} {}^{q}m_S = {}^{q-1}m_S + \Delta m_S \\ {}^{q}\mathbb{Y}_0 = {}^{q-1}\mathbb{Y} \\ \Phi({}^{q}\mathbb{Y}; {}^{q}m_S) = 0. \end{cases} \tag{47}$$

The choice for the value Δm_S deserves further discussion. A constant increment Δm_S turns out to increase the computational effort since ${}^{1}m_S = 0$ while the final value of $m_S = 3.2890 \times 10^5$. An appropriate method for generating a non-uniform spacing of the continuation parameter m_S is to expand the current value ${}^{q-1}m_S$ according to the relation ${}^{q}m_S = c\, m_S^{q-1}$ such that ${}^{q}m_S = {}^{1}m_S c^{q-1}$ with $c > 1$—but for $q = 2$ where the increment of Eq. 47 is used.

Figure 3 shows the sample solution of Fig. 1 continued under four-body dynamics. For this case $N = 101$ points are assumed; five intermediate BVPs, which increase m_S by one order of magnitude ($c = 10$), were necessary for convergence. The number of Newton iterations ranges from three to eight, and the total computational time for this orbit is 5 s. The termination tolerance ε (cfr. Eq. 42) was "relaxed" for the first steps and then set equal to 10^{-10} for the last one. The initial value taken for the phase of the Sun accordingly to equation set (13) is $\theta_0 = 0$.

In analogy with the previous section, the whole L_1 and L_2 families of halo orbits, which are governed by four-body dynamics, have been computed (Fig. 4). Each orbit is amplitude-parameterized by A_z. Furthermore, supplying p-periodic initial guesses, it is possible to compute quasi-periodic solutions orbiting p-times about the substitute of the equilibrium point. An example is illustrated in Fig. 5 in which an L_2 quasi-periodic halo performs four revolutions. Nevertheless, such kinds of solutions require an elevated computational effort because, as mentioned before, the Sun's perturbations act

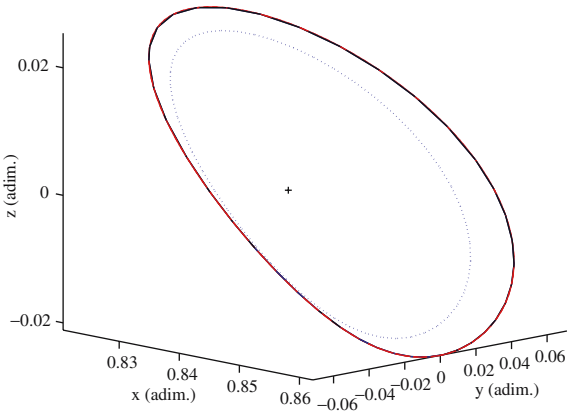

Fig. 3 L_1 halo orbit of Fig. 1 continued in the R4BP; orbit of Fig. 1 (dotted), LMPM solution (dash-dot) and RKF78 validation (solid)

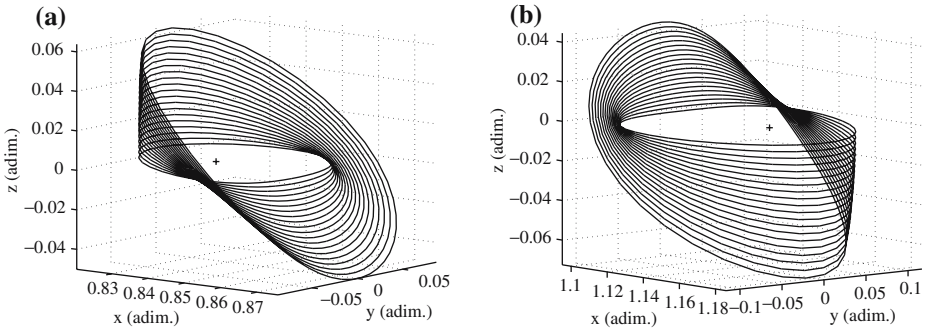

Fig. 4 Families of quasi-periodic halo orbits around the substitutes of L_1 and L_2 under the R4BP dynamics. (**a**) L_1 family; (**b**) L_2 family

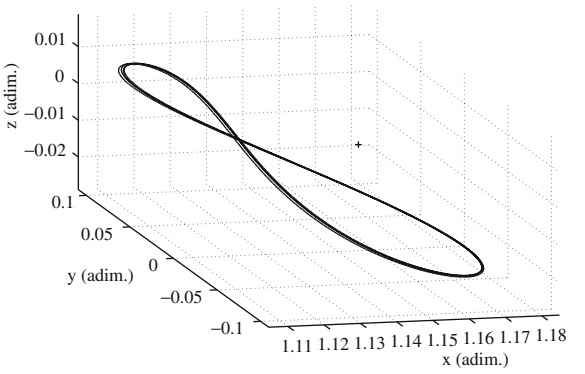

Fig. 5 A four-revolution quasi-periodic Sun-perturbed orbit about the L_2 substitute

to break the periodicity of the L_2 halos. For example, the solution shown in Fig. 5 has been computed using $N = 10,000$ points (which means $nN = 80,000$ variables in this case) and its computation has been possible using the efficient factorization algorithm reported in the appendix.

4.3 Optimal low thrust transfer to a L_1 halo

As stated in Sect. 2.1, L_1 and L_2 represent hyperbolic equilibrium points, and so they give rise to two invariant one-dimensional subsets: the stable and unstable manifolds ($W^{s,u}_{L_i}$, $i = 1,2$). This characteristic holds also for the periodic orbits about such points, but for this case two-dimensional stable and unstable manifolds ($W^{s,u}_{Li.p.o.}$, $i = 1,2$) exist. For example, Fig. 6 shows the interior branch of the stable manifold associated to a $A_z = 8,000$ km L_1 halo orbit of Fig. 1 (Bernelli-Zazzera et al. 2004).

Stable manifolds associated with the halo orbits are of particular interest in mission design since the dynamical system (1) by itself will bring a spacecraft placed on this manifold toward the orbit without using propellant. Hence, the optimal control problem illustrated in Sect. 2.5 is rewritten in terms of $\mathbf{y}$ and $\boldsymbol{\lambda}$, based on Eq. 18,

$$\begin{cases} \dot{\mathbf{y}} = \mathbf{f}(\mathbf{y}, \boldsymbol{\lambda}) \\ \dot{\boldsymbol{\lambda}} = -\left(\dfrac{\partial \mathbf{f}}{\partial \mathbf{y}}\right)^T \boldsymbol{\lambda}, \end{cases} \tag{48}$$

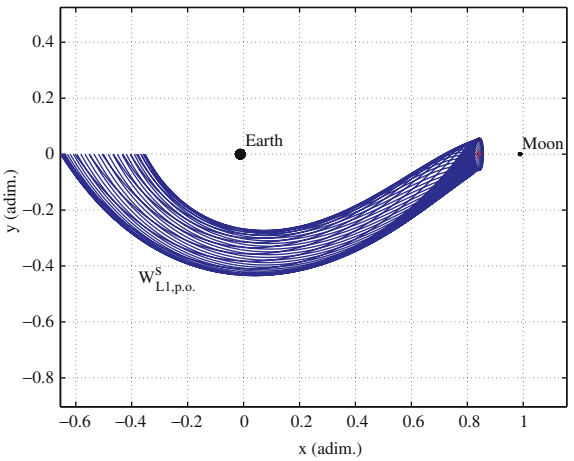

Fig. 6 Interior branch of the $W^s_{L_1,p.o.}$ (Bernelli-Zazzera et al. 2004)

and it must be solved with the two-point conditions

$$\begin{cases} \mathbf{y}(t_0) = \mathbf{y}_0 \\ \mathbf{y}(t_f) = \mathbf{y}_f, \end{cases} \tag{49}$$

in which $\mathbf{y}_f \in W^s_{L_1,p.o.}$. In other words, the final point $\mathbf{y}_f$ of the controlled leg must lie on the stable manifold associated to the periodic orbit in the phase space sense (i.e. position and velocity). The initial time t_0 and the initial state $\mathbf{y}_0$ are properly chosen on a tangential thrust spiral starting from the perigee of a $200 \times 36{,}000$ km GTO orbit. The final time t_f has been selected to be consistent with the choice of initial conditions.

Figure 7 shows an example of the solution to the optimal control problem stated above. After the tangential thrust leg, which determines the initial point $\mathbf{y}_0$, the BVP (48) and (49) is solved, and the right boundary condition sets the point $\mathbf{y}_f$ to lie on the stable manifold branch. The solution has been validated using a RKF78 integration scheme and a cubic spline interpolation of the optimal control values. The algorithm has been able to converge using $N = 1{,}001$ grid points.

The initial tangential thrust $u = 2 \times 10^{-4}$ m/s^2 acts for a time equal to t_0. Its value is an order of magnitude greater than the optimal control law, reported in Fig. 8a, and contributes mostly to the computation of the propellant mass fraction necessary for the transfer, defined by the rocket equation as

$$f = \frac{m_p}{m_0} = 1 - \mathrm{e}^{-\frac{\int_0^{t_0} \|\mathbf{u}(t)\| \mathrm{d}t}{I_{sp} g_0}}. \tag{50}$$

To derive f, a specific impulse $I_{sp} = 3{,}000$ s is assumed. Table 1 summarizes a set of five solutions found in terms of time interval, propellant mass fraction, and total time of flight (TOF), which includes the tangential thrust spiral, the optimal leg, and the stable manifold branch. The first row corresponds to the solution of Fig. 7.

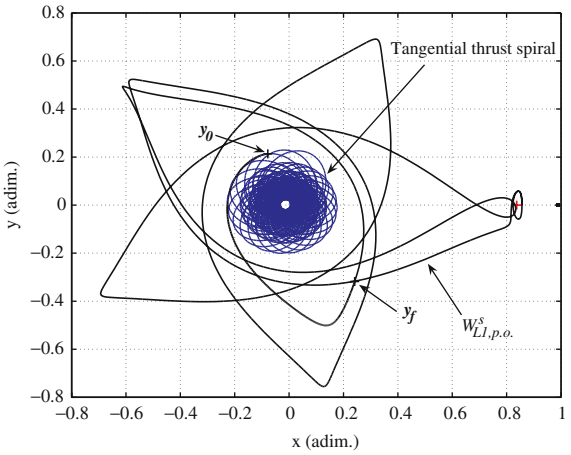

Fig. 7 An example of the solution to the optimal control problem; tangential thrust spiral (solid), solution with the LMPM and RKF78 + cubic spline validation (bold); stable manifold leg and L_1 periodic orbit (solid)

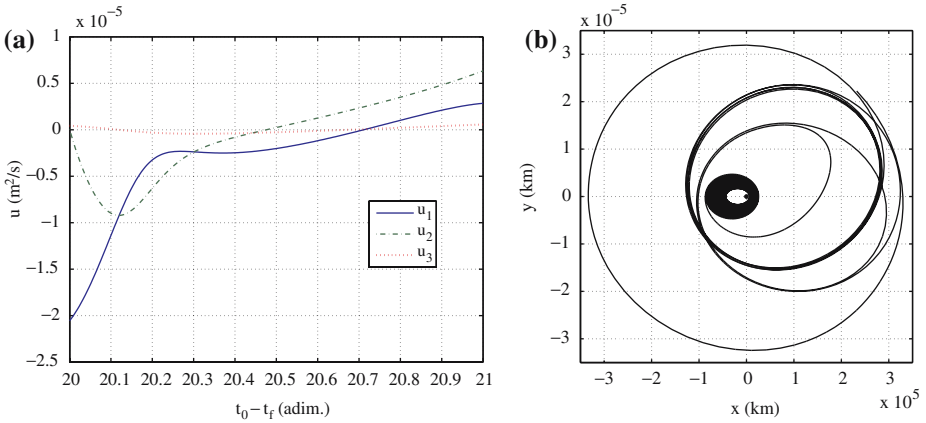

Fig. 8 Optimal thrust profile and low thrust transfer trajectory relative to the solution of Fig. 7. (**a**) optimal control law; (**b**) trajectory in the Earth-centered frame

Table 1 Solutions found for the low thrust optimal control problem

f (adim.)	t_0 (adim.)	t_f (adim.)	TOF (days)
0.0498	20	21	188.5
0.0498	20	22	192.9
0.0618	25	28	219.0
0.0737	30	31	232.0
0.0855	35	36	253.7

5 Final remarks

A linear multi-point method has been applied for the solution of several representative boundary value problems in astrodynamics. This method is based on the discretization of the problem on a uniform grid by means of a sixth-order accurate

scheme. In practice, the proposed formulation expresses the solution of the BVP in first-order form, and it becomes an ordinary matter of numerical non-linear algebra. Simultaneously, the profile of the block matrices is *bordered quadri-diagonal*, and this structure can be easily preserved by properly choosing the direction in the factorization and elimination process.

Such a solution scheme has been applied to generate halo orbits from both the restricted three- and four-body problems. While in the former case the families of L_1 and L_2 halo orbits have been easily computed, the latter required a numerical continuation method for convergence. Thanks to numerical efficiency, each BVP has been solved in fractions of a second. Furthermore, the LMPM has been applied to solve an open problem in astrodynamics (Senent et al. 2005) concerning the design of trajectories reaching the halo orbits by combining low thrust and invariant manifolds. The associated optimal control problem, stated by the Euler–Lagrange system of equations, have been solved comfortably.

Finally, in Fig. 9 the error values versus grid-point number is shown. Since the analyzed problems do not have any analytical solutions, the error can be defined as $e = |\mathbf{y}_N - \tilde{\mathbf{y}}_f|_\infty$ where $\tilde{\mathbf{y}}_f = \varphi(t_0, t_f, \mathbf{y}_1)$ is the solution at time t_f flowed with the RKF78 integrator (relative and absolute tolerance set to 10^{-12}) starting from $(t_0, \mathbf{y}_1)$. In this context $\mathbf{y}_1$ and $\mathbf{y}_N$ represent the unknowns corresponding, respectively, to first and to the final mesh point. The maximum distance, in the phase space sense, between the solution given by LMPM and the validated orbit in Fig. 1 is $e = 5.85\ 10^{-8}$ ($N = 51$), while the maximum error of the solution in Fig. 3 is $e = 3.07\ 10^{-7}$ ($N = 101$). The optimal control problem has been validated with the same integration method which implements a cubic interpolation of the control force history $\mathbf{u}_i$, $i = 1, \ldots, N$. The solution in Fig. 7 ($N = 1,001$) has a final error equal to $e = 4.41\ 10^{-9}$ which is much less than the thrust level.

We conclude by emphasizing once more the extreme efficiency, flexibility and reliability of the proposed method which is based on an algebraic transcription of the original differential problem.

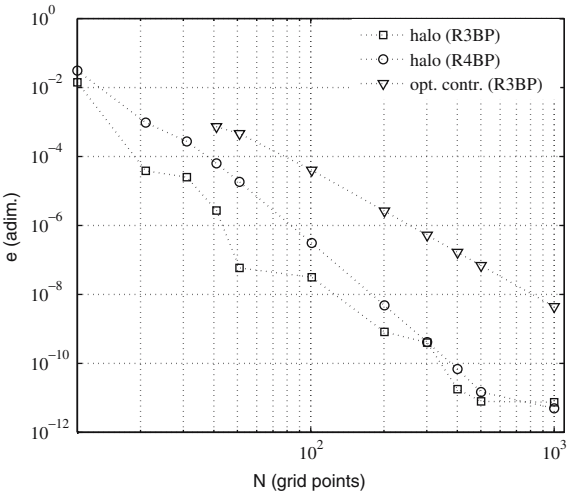

Fig. 9 The points (N, e) relative to the three astrodynamics application discussed in the previous sections

Acknowledgements The authors are strongly indebted to Prof. Luigi Quartapelle for his passionate collaboration and for sharing his effective software.

Appendix

Algorithmic flow chart

For the sake of clarity we report below the algorithmic flow chart summarizing the process to solve the discussed BVPs. Equation numbers refer to those introduced throughout the paper (Fig. 10).

Factorization of the bordered quadri-diagonal matrix

The solution $\Delta\mathbb{Y}_k$ at the k iteration is given by $\Delta\mathbb{Y}_k = \mathbb{A}_k^{-1}\boldsymbol{\varphi}(\mathbb{Y}_k)$ and is determined by a UL block factorization of the matrix of the system, $\mathbb{A}_k = \mathbb{U}_k\mathbb{L}_k$. The adoption of the UL factorization proceeding from the bottom right corner in place of the more classical UL factorization is needed to avoid the fill-in of the zero triangle comprised between the first row and the band of the matrix.

The matrix $\mathbb{A}_k$ of this system has the block bordered quadri-diagonal profile, with four extra-band elements associated with the two special computational molecules based on five points at the interval extremes. The profile of the block matrix associated with the $O(h^6)$ LMPM is given for completeness

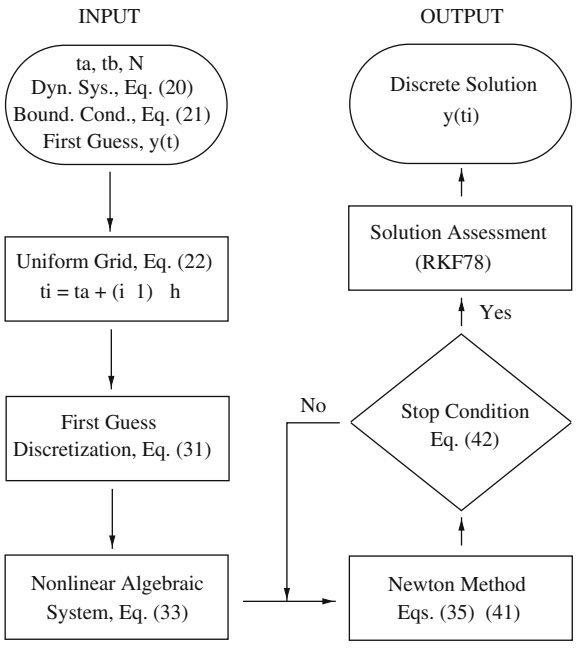

Fig. 10 Algorithm flow chart used to solve the BVPs discussed in the paper

$$\mathbb{A}_k = \begin{bmatrix}
G_1 & G_2 & G_3 & G_4 & G_5 & \cdot & \cdot & \cdot & G_{N-2} & G_{N-1} & G_N \\
B_1 & C_2 & D_3 & \hat{D}_2 & \hat{D}_1 & & & & & & \\
A_1 & B_2 & C_3 & D_4 & & & & & & & \\
 & A_2 & B_3 & C_4 & D_5 & & & & & & \\
 & & A_3 & B_4 & C_5 & D_6 & & & & & \\
 & & & \cdot & \cdot & \cdot & \cdot & & & & \\
 & & & & \cdot & \cdot & \cdot & \cdot & & & \\
 & & & & & \cdot & \cdot & \cdot & \cdot & & \\
 & & & & & & A_{N-4} & B_{N-3} & C_{N-2} & D_{N-1} & \\
 & & & & & & \hat{B}_N & A_{N-3} & B_{N-2} & C_{N-1} & D_N \\
 & & & & & & \hat{A}_N & \hat{A}_{N-1} & A_{N-2} & B_{N-1} & C_N
\end{bmatrix}.$$

Notice the four extra quadri-diagonal blocks for the first and last special molecule, with five points stored as blocks $\hat{D}_2, \hat{D}_1, \hat{A}_N$ and $\hat{A}_{N-1}$ to exploit the first two and last two available unused entries of the block diagonals D_i and A_i, respectively. Notice furthermore that in the matrix profile an additional block $\hat{B}_N$ has been added to the second last row. This block is initially empty but must be retained in the matrix profile since the block factorization process fills-in this position with non-zero values. We wish to emphasize that the first row of $\mathbb{A}_k$ represents the discretized boundary conditions. This row is non-zero if integral boundary conditions are supplied; otherwise only G_1 and G_N are full.

The factorization algorithm produces the block, bordered upper-bi-diagonal matrix and block lower-tri-diagonal matrix below

$$\mathbb{U} = \begin{bmatrix}
\mathcal{G}_1 & \mathcal{G}_2 & \mathcal{G}_3 & \mathcal{G}_4 & \mathcal{G}_5 & \cdot & \cdot & \cdot & \mathcal{G}_{N-2} & \mathcal{G}_{N-1} & \mathcal{G}_N \\
 & \mathcal{C}_2 & \mathcal{D}_3 & \hat{\mathcal{D}}_2 & \hat{\mathcal{D}}_1 & & & & & & \\
 & & \mathcal{C}_3 & \mathcal{D}_4 & & & & & & & \\
 & & & \mathcal{C}_4 & \mathcal{D}_5 & & & & & & \\
 & & & & \mathcal{C}_5 & \mathcal{D}_6 & & & & & \\
 & & & & & \cdot & \cdot & & & & \\
 & & & & & & \cdot & \cdot & & & \\
 & & & & & & & \cdot & \cdot & & \\
 & & & & & & & & \mathcal{C}_{N-2} & \mathcal{D}_{N-1} & \\
 & & & & & & & & & \mathcal{C}_{N-1} & \mathcal{D}_N \\
 & & & & & & & & & & \mathcal{C}_N
\end{bmatrix}$$

$$\mathbb{L} = \begin{bmatrix} I & & & & & & & & \\ \mathcal{B}_1 & I & & & & & & & \\ \mathcal{A}_1 & \mathcal{B}_2 & I & & & & & & \\ & \mathcal{A}_2 & \mathcal{B}_3 & I & & & & & \\ & & \mathcal{A}_3 & \mathcal{B}_4 & I & & & & \\ & & & \ddots & \ddots & & & & \\ & & & & \ddots & \ddots & & & \\ & & & & & \ddots & \ddots & & \\ & & & & & \mathcal{A}_{N-4} & \mathcal{B}_{N-3} & I & \\ & & & & & \hat{\mathcal{B}}_N & \mathcal{A}_{N-3} & \mathcal{B}_{N-2} & I \\ & & & & & \hat{\mathcal{A}}_N & \hat{\mathcal{A}}_{N-1} & \mathcal{A}_{N-2} & \mathcal{B}_{N-1} & I \end{bmatrix}.$$

References

Battin, R.H.: An Introduction to the Mathematics and Methods of Astrodynamics. AIAA, New York (1987)

Bernelli-Zazzera, F., Topputo, F., Massari, M.: Assessment of Mission Design Including Utilization of Libration Points and Weak Stability Boundaries. Final Report, ESTEC Contract No. 18147/04/NL/MV (2004)

Bryson, A.E., Ho, Y.C.: Applied Optimal Control. John Wiley & Sons, New York (1975)

Fox, L.: The Numerical Solution of Two-Point Boundary Value Problems in Ordinary Differential Equations. Oxford University Press, Oxford (1957)

Gómez, G., Jorba, Á., Masdemont, J., Simó, C.: Dynamics and Mission Design near Libration Points—Volume III: Advanced Methods for Collinear Points. World Scientific (2000)

Lambert, J.D.: Numerical Methods for Ordinary Differential Systems: The Initial Value Problem. Wiley, Chichester (1991)

Masdemont, J.J.: High order expansions of invariant manifolds of libration point orbits with applications to mission design. Dyn. Sys.: An Int. J. **20**, 59–113 (2005)

Masdemont, J., Mondelo, J.M.: Notes for the Numerical and Analytical Techniques Lectures. Advanced Topics in Astrodynamics, Barcelona (2004)

Quartapelle, L., Rebay, S.: Numerical solution of two-point boundary value problems. J. Comput. Phys. **86**, 314–354 (1990)

Quartapelle, L., Scandroglio, A.: Solution of the Falkner-Skan Equation to Determine Reverse Flow. DIA-SR 03-05 (2003)

Richardson, D.L.: Halo orbit formulation for the ISEE-3 mission. J. Guid. Contr. **3**, 543–548 (1980)

Senent, J., Ocampo, C., Capella, A.: Low-thrust variable-specific-impulse transfers and guidance to unstable periodic orbits. J. Guid. Contr. Dyn. **28**, 280–290 (2005)

Simó, C., Gómez, G., Jorba, Á., Masdemont, J.: The bicircular model near the triangular libration points of the RTBP. In: Roy, A.E., Steves, B.A. (eds.) From Newton to Chaos, pp. 343–370. Plenum Press, New York (1995)

Stoer, J., Bulirsch, R.: Introduction to Numerical Analysis. Springer, New York (1993)

Szebehely, V.: Theory of Orbits: The Restricted Problem of Three Bodies. Academic Press Inc., New York (1967)

Thurman, R., Worfolk, P.: The Geometry of Halo Orbits in the Circular Restricted Three-Body Problem. Geometry Center Research Report, University of Minnesota, GCG95 (1996)

Yagasaki, K.: Sun-perturbated earth-to-moon transfers with low energy and moderate flight time. Celest. Mech. Dyn. Astr. **90**, 197–212 (2004)